Periodic superradiance in an Er:YSO crystal

Hideaki Hara [1,*] Junseok Han [1,2] Yasutaka Imai [1] Noboru Sasao,[1] Akihiro Yoshimi [1] Koji Yoshimura [1]
Motohiko Yoshimura,[1] and Yuki Miyamoto [1,†]

[1]*Research Institute for Interdisciplinary Science, Okayama University, Okayama 700-8530, Japan*
[2]*Department of Physics and Astronomy & Institute of Applied Physics, Seoul National University, Seoul 08826, Korea*

We observed periodic optical pulses from an Er:YSO crystal during irradiating with a continuous-wave excitation laser. We refer to this phenomenon as "periodic superradiance." This periodicity can be understood qualitatively by a simple model, in which a cyclic process of a continuous supply of population inversion and a sudden burst of superradiance is repeated. The excitation power dependences of peak interval and the pulse area can be interpreted with our simple model. In addition, the linewidth of superradiance is much narrower than an inhomogeneous broadening in a crystal. This result suggests that only Er^{3+} ions in a specific environment are involved in superradiance.

I. INTRODUCTION

A considerable number of theoretical and experimental studies on superradiance (SR) have been conducted, starting with the prediction by Dicke in 1954 [1]. If a correlation between the atomic or molecular dipole moments is generated, the peak transition rate is accelerated and becomes proportional to N^2 because a macroscopic dipole proportional to the number of atoms N is created. When SR starts from uncorrelated fully excited states, it is sometimes called superfluorescence, but in this paper we refer to all such phenomena as SR in a broad sense [2]. For SR to occur, this macroscopic dipole has to develop within a decoherence time T_2 and a population inversion has to reach a certain threshold. So far SR has been demonstrated in gases [3–5] and solid-state materials [6–9].

Recently, SR was observed from Er^{3+} ions doped in a Y_2SiO_5 crystal (Er:YSO) [10]. The intraconfiguration $4f \rightarrow 4f$ transitions of rare-earth ions doped into crystals has remarkably long decoherence time despite being in a solid environment because $4f$ electrons are shielded by $5s$ and $5p$ shells from interactions with the host lattice. An Er:YSO crystal exhibits a narrowest homogeneous linewidth of 73 Hz in a solid [11]. Various applications toward quantum information processing [12–14] and fundamental physics [15–17] have been proposed.

In this paper, we report on experimental studies of SR with a quasiperiodic time structure observed in an Er:YSO crystal.

In past SR experiments, usually a single SR pulse, with or without ringing, is generated after an excitation by a pulsed laser. In contrast, observed pulses in the present case are generated periodically while the continuous-wave (CW) excitation laser is turned on. In Ref. [10], SR pulses in an Er:YSO crystal are persistent under a CW excitation. However, no attention was paid to the periodicity. It is not obvious that the persistent SR pulses are generated periodically. In addition, the linewidth of the observed SR is found to be comparable to the Fourier limit, much narrower than an inhomogeneous broadening in a crystal. In this paper we especially focus on the periodicity and linewidth of SR pulses.

Since the quasiperiodic nature of the SR pulses appears to stand in sharp contrast to the stochastic nature of conventional SR, it is important to understand how coherence is developed periodically by a CW excitation. If coherence development becomes more controllable by, for example, a trigger laser, various application possibilities will open up [15–17]. It is also interesting to investigate the linewidth of SR because it might shed light on the interaction between a laser and Er dopants in a crystal environment. Generating narrow linewidth optical pulses for an input of a CW excitation laser is expected to be of practical importance.

Below we describe the results of our experiment, focusing on the periodic nature. A simple model is also given which treats it as repetition of a cyclic process of a continuous supply of population inversion and a sudden burst of SR emissions after reaching an SR threshold.

II. EXPERIMENTAL SETUP

Figure 1(a) shows the energy diagram of Er^{3+} ions doped in a YSO crystal. Each state is split into several Stark levels by the crystal field. Er^{3+} ions are excited from the ground state to the lowest Stark level of the $^4I_{9/2}$ state with a wavelength of 808 nm. The excited Er^{3+} ions rapidly decay via nonradiative processes. In this way the population accumulates in the
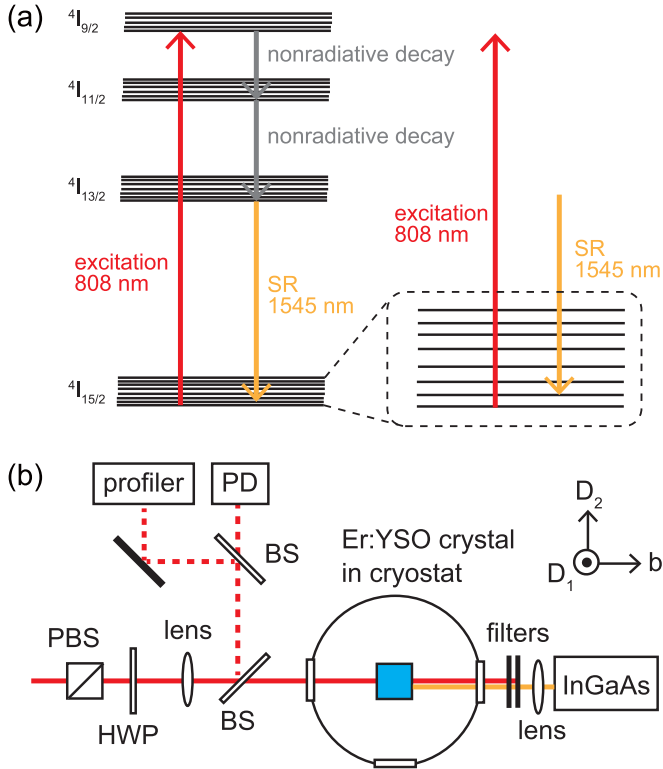
FIG. 1. (a) Energy diagram of Er^{3+} ion doped in YSO crystal. The dashed rounded square shows an enlarged view of the $^4I_{15/2}$ ground state. (b) Experimental setup. PBS; polarization beam splitter. HWP; half-wave plate. BS; beam sampler. PD; photodetector. InGaAs; InGaAs photodetector.

lowest Stark level of the $^4I_{13/2}$ state with a long lifetime, which is measured by the fluorescence (spontaneous emission) to be roughly 10 ms. Besides the fluorescence, the optical pulses propagating in the forward direction are generated.

Figure 1(b) shows the experimental setup. The target is an Er^{3+}:YSO crystal grown by Scientific Materials, Inc. of Bozeman, Montana. The Er^{3+} ions at site 2 are used in our experiment. The number density of Er^{3+} ions at each site is roughly 5×10^{18} cm^{-3} according to the nominal concentration value of 0.1%. The crystal is held by a copper holder in a cryostat and it is cooled to roughly 4 K by a Gifford-McMahon refrigerator. Almost all the Er^{3+} ions exist in the lowest Stark level of the $^4I_{15/2}$ ground state at 4 K. The crystal is aligned with the laser k vector parallel to the b axis along a 6 mm path. Other crystal dimensions are 4 mm along the D_1 axis and 5 mm along the D_2 axis. The polarization of the input laser is parallel to the D_2 axis. The beam diameter ($2w_0$) is loosely focused on the crystal to roughly 300 μm and it remains almost unchanged in the crystal. The input laser power is monitored by a photodetector and it is typically 90 mW. The laser position is also monitored by a beam profiler. An indium-gallium-arsenide (InGaAs) photodetector (HCA-S-200M-IN; FEMTO Messtechnik GmbH) detects generated optical pulses. The residual excitation laser is removed by long pass filters in front of the detector.

The time sequence of the laser excitation of Er^{3+} ions is controlled by an acousto-optic modulator (AOM). The exci-
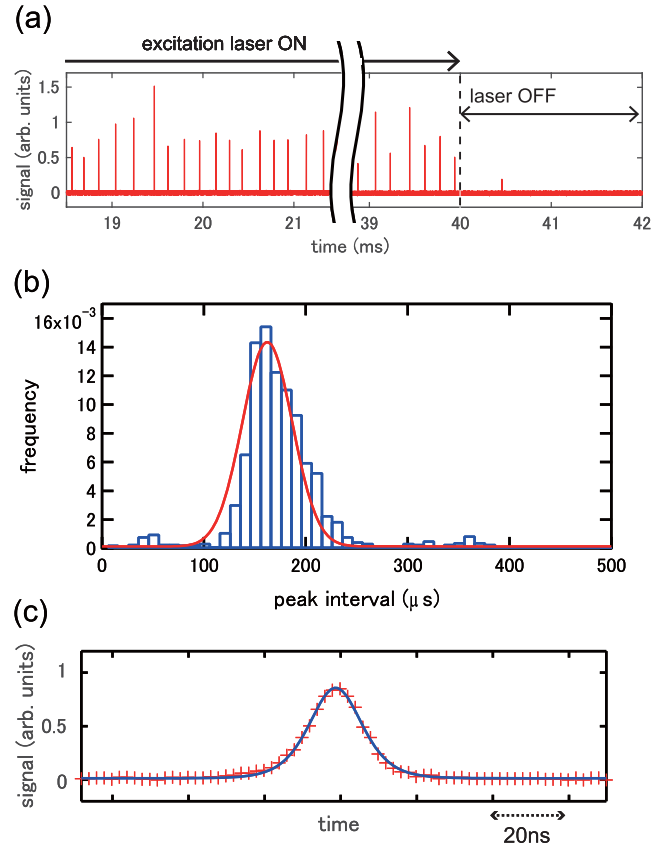

FIG. 2. (a) Example of waveform of observed periodic pulses in the middle 3 ms of excitation and from 1 ms before the excitation laser is turned off. The excitation laser is turned on for 40 ms from $t = 0$. (b) Histogram of the peak interval between neighboring pulses. The red line is the Gaussian fit. (c) Example of observed single pulse. The red crosses are the data points. The blue solid line is the fit by a sech-squared function.

tation laser is turned on for 40 ms every 200 ms: this time sequence is chosen in such a way that the duration of the excitation laser is much longer than the observed pulse duration and period, and at the same time the temperature rise of the target crystal, which shortens the decoherence time, is low enough. The 40 ms excitation data is taken ten times repeatedly.

III. RESULTS AND DISCUSSION

We observed a train of light pulses: the pulses begin to appear several ms after the laser is turned on ($t = 0$), and disappear, or at most one SR pulse is generated right after it is turned off ($t = 40$ ms). Figure 2(a) shows an example of the observed pulses in the middle 3 ms of the excitation and from 1 ms before the excitation laser is turned off, respectively. The pulses are generated at almost constant time intervals, in other words, periodically. Figure 2(b) is a histogram of peak intervals, which are defined by the time difference between adjacent peaks (the data after $t = 10$ ms are plotted, where the system has reached equilibrium). The red line is the Gaussian fit. The mean period and the standard deviation given by the fit are 160 μs and 20 μs, respectively. The pulses are generated in

the transition from the lowest Stark level of the $^4I_{13/2}$ state (lifetime: $\sim$10 ms) to the second lowest Stark level of the $^4I_{15/2}$ ground state (lifetime: $\sim$ 400 ns, see Appendix A for more details). It is confirmed by a monochromator and the wavelength of the pulses is $\lambda = 1545$ nm.

The observed pulses are identified as SR based on the following observations: (i) short pulse duration, (ii) sech-squared pulse shape, (iii) relationship between pulse duration and height, and (iv) relationship between pulse area and height. Below we elaborate these points in more detail. Figure 2(c) is a typical example of a single observed pulse (the red crosses). The FWHM (full-width-half-maximum) pulse duration of such pulses are observed to fluctuate with the mean duration of 20 ns and the standard deviation of 5 ns, respectively. They are given by the Gaussian fit to the histogram of the duration. The observed pulse duration is 10^6 times shorter than the lifetime of the higher state of this transition ($\sim$10 ms), whereas it is consistent with an expected time scale of SR. Actually, the characteristic time of SR is given in a simplified two-level model by [2]

$$T_R = 8\pi/(3\gamma N_0 \lambda^2 L), \qquad (1)$$

where N_0 denotes a number density of Er^{3+} ions related to SR, λ is a wavelength of SR (1545 nm), L is a sample length (6 mm), and γ is a radiative decay rate. An approximate value of T_R may be estimated as follows. For $N_0(=N/V)$, we use the number of photons N in a single pulse divided by the excitation volume V. Here N is not the total Er^{3+} ion number because the effective number of the Er^{3+} ions related to SR is not clear. $N \simeq \mathcal{O}(10^{12})$ is estimated from the measured signal pulse area with the efficiency of the InGaAs photodetector, and the transmittance of the filters, and V is taken to be L times the laser beam cross section (πw_0^2). The upper limit of γ is given by the lifetime of the higher state multiplied by the radiative branching ratio to the lower states [18], and is found to be 40 Hz. Combining these factors, T_R is calculated to be longer than $\mathcal{O}$ (1 ns). Considering a numerical factor needed to convert T_R to the pulse duration and ambiguity in γ, we conclude that our observed pulses are consistent with SR.

For our experimental configuration, it is expected that the macroscopic polarization (coherence) develops homogeneously over the target ($L \ll cT_R$), and thus SR pulse shapes become sech-squared function [19]. As shown by the blue solid line in Fig. 2(c), the observed pulse shape is indeed well fit by this function. It is also expected that the pulse duration is inversely proportional to the square root of the peak height since the former is proportional to $T_R \propto 1/N$ [Eq. (1)], and the latter to N^2. Similarly the pulse area ($\propto N$) is proportional to the square root of the peak height. These relationships are examined by the data and found to hold approximately (see Appendix B for more details).

The periodic behavior of the observed SR can be interpreted with the following simple model. (i) The excitation laser pumps up Er^{3+} ions to the higher state of the SR transition. (ii) A part of them deexcites to the lower states via spontaneous emissions. (iii) During the process, macroscopic polarization (coherence) also develops, until it reaches the SR threshold. (iv) Then, the population of the higher state (also the coherence) suddenly decreases, resulting in a sharp pulse.
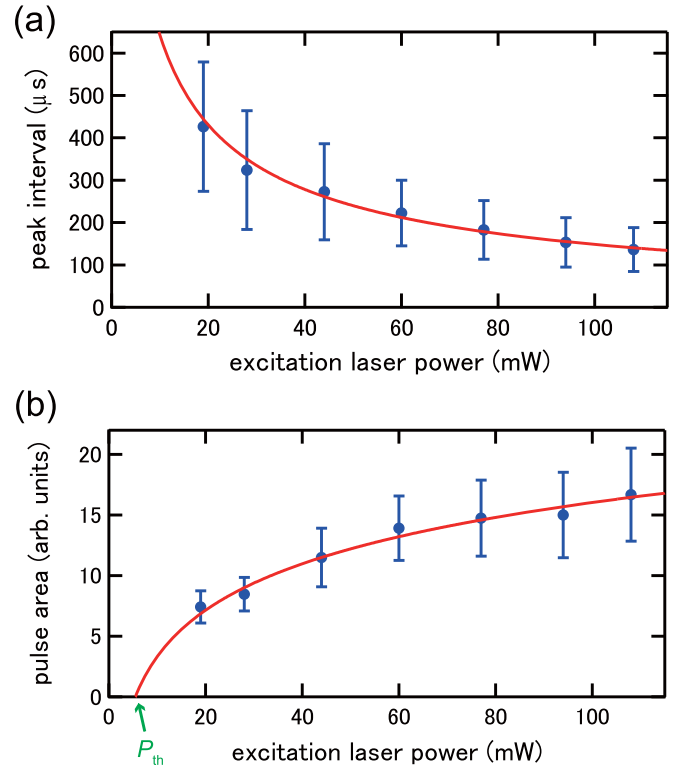

FIG. 3. (a) Peak interval at various excitation laser power. The blue circles represent the averages. The error bars indicate the standard deviations, not the statistical errors. The red line is the fit of (interval) $= A \times \ln(P/P_{th})/(P - P_{th})$ to the data. (b) Pulse area at various excitation laser power. The blue circles and the error bars indicate the averages and the standard deviations, respectively. The red line is the fit of (area) $= B \times \ln(P/P_{th})$ to the data. The threshold power P_{th} is common to both fits.

(v) The population of the lower state of SR decays to the ground state immediately. (vi) By repeating these processes, the periodic SR pulses are generated. As mentioned above, the measured lifetime of the higher and lower states of SR are roughly 10 ms and 400 ns, respectively. The lifetime of the lower state of SR is short enough to generate the population inversion. It does not limit T_2 to a short value, and is long enough to generate SRs. Our simple model is indeed qualitative and a more quantitative model is necessary to fully explain the behavior of the periodic SR. However, the overall picture of the observed phenomenon can be understood by our simple model.

To confirm the validity of our model, we investigated the dependence on the excitation laser power. Figures 3(a) and 3(b) show, respectively, the peak interval and pulse area as a function of the excitation laser power. All the observed pulses in 40 ms are used in this analysis. As the power increases, the period gets shorter and the area becomes larger. The solid lines in Figs. 3(a) and 3(b) are the results of fits whose functional forms are derived from our model plus the assumption that the SR threshold (thus, T_R) is independent of the laser power. Since the coherence buildup is a competing process between pumping and deexcitation rates, there should exist some threshold intensity I_{th} for the excitation laser. The actual laser beam is not uniform spatially but has a radius
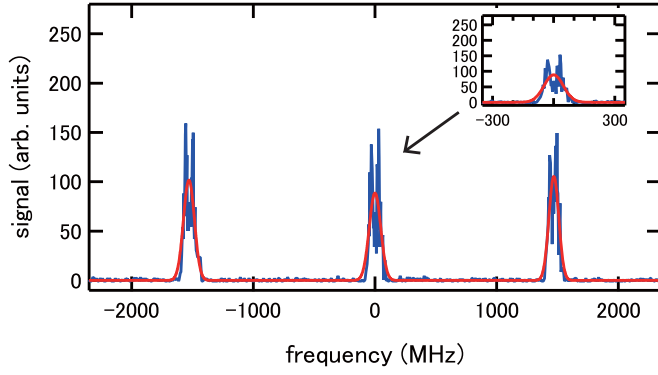
FIG. 4. Linewidth measurement of SR using a confocal cavity. The cavity length is scanned by changing a PZT voltage. The red line is the Gaussian fit. The inset shows an enlargement of one of the peaks.

dependence. Thus, an effective area in which the intensity exceeds I_{th} should increase as the laser power. Assuming a Gaussian intensity profile $I(r) = I_0 \exp(-2r^2/w_0^2)$, we expect the effective volume $V_{eff} = \pi r_{th}^2 L$ also increases as $\ln(I_0/I_{th})$. Here, $I_0 = 2P/\pi w_0^2$ is a peak intensity for the excitation laser power P and r_{th} is a threshold radius determined by $I(r_{th}) = I_{th}$. From the constancy of T_R or $N_0 = N/V_{eff}$, not N/V here, we expect N (proportional to the pulse area) to increase as $\ln(I_0/I_{th})$. The peak interval, on the other hand, is inversely proportional to the intensity averaged over the cross sectional area πr_{th}^2 in our model: thus we expect it is proportional to $\ln(I_0/I_{th})/(I_0 - I_{th})$. Actual fits to the data, both peak interval and pulse area, are done simultaneously using (interval) $= A \times \ln(P/P_{th})/(P - P_{th})$ and (area) $= B \times \ln(P/P_{th})$ with A, B, and P_{th} as free parameters. The threshold power P_{th} has a relationship of $I_{th} = 2P_{th}/\pi w_0^2$ with I_{th}. The measured results are fit well by using our model. The fitting results give $P_{th} = 5.5 \pm 0.6$ mW. This error is scaled so that the reduced χ^2 value is unity. The value of P_{th} is consistent with the experimental fact that no periodic SR can be observed below 10 mW. The above results of the excitation laser power dependence support the validity of our model.

Self-pulsing of the laser is also a well-known phenomenon where persistent pulses are generated under a CW excitation [20]. The periodic SR we observed is a new phenomenon that, different from self-pulsing, is triggered by development of coherence among ensembles.

IV. LINEWIDTH OF SR

We now focus on the linewidth of SR. For this measurement, the SR pulses coming out of the crystal are coupled to an optical fiber, which is in turn sent to a confocal cavity (SA200-14A; Thorlabs) whose Finesse and free spectral range (FSR) are >200 and 1.5 GHz, respectively. While the cavity length is swept over 3 FSR slowly (at 0.013 Hz) by changing the PZT voltage, the light intensity transmitted from the cavity is measured by the same photodetector as in the SR experiment. Figure 4 is an example of the transmitted signal vs the cavity length. The red line is the Gaussian fit, which gives the FWHM linewidth of 100 MHz when averaged over three peaks. Several comments are in order here. First,

the actual linewidth may be much narrower than the quoted value because it contains shot-by-shot frequency fluctuations of the SR pulse. In fact, the measured linewidth is broader than its Fourier limit, $\sim$20 MHz, which is estimated from the observed pulse width of $\sim$20 ns. Second, the measured width turns out to be much narrower than the typical inhomogeneous broadening in the crystal ($\sim$1 GHz). We do not measure the inhomogeneous broadening of the SR transition. The linewidth of the transition from the ground state to the lowest Stark level of the $^4I_{13/2}$ state is measured to be roughly 1 GHz. The inhomogeneous broadening of the SR transition is expected to be similar to 1 GHz. The result of the narrow linewidth indicates that only the Er^{3+} ions in a specific environment with a narrow frequency range are involved in SR. We believe that the periodic nature of observed SR pulses is deeply related to this feature.

V. INHOMOGENEITY OF CRYSTAL

As a point of caution, the period changes depending on the excited region of the crystal due to inhomogeneity. It is confirmed by changing the alignment of the excitation laser. However, the periodic behavior can be reproduced if the alignment is adjusted properly. Even if the period itself changes, the various properties of the periodic pulses can be discussed in the same way as above at other regions of the crystal.

VI. CONCLUSION

In summary, we observed a phenomenon which can be characterized as a periodic SR in an Er:YSO crystal. The periodic time structure can be understood by our simple model, which presumes that the periodic SR is generated in a cyclic process of continuous population inversion and a sudden burst of SR emissions initiated at the SR threshold. The validity of our model is supported, at least partially, by the results of the power dependence measurements. The model is admittedly qualitative: if more quantitative understanding is succeeded in, the control of the temporal behavior of the SR can be realized in the future. In addition to these features above, we revealed that, from the linewidth measurement, a narrow transition frequency range is selected for SR pulses within an inhomogeneous broadening. We believe that this is one of the key features to realize the periodic time structure. The periodic SR we observed also presents a potential as a light source, where narrow linewidth optical pulses are generated in a simple system without injection seeding. Coherent phenomena in a solid have possible applications towards quantum information processing [12–14] and fundamental physics [15–17]. Understanding and controlling coherent phenomena will play an important role in these research fields.

APPENDIX A: LIFETIME OF THE LOWER STATE OF SUPERRADIANCE

The SR pulses are generated in the transition from the lowest Stark level of the $^4I_{13/2}$ state to the second lowest Stark level of the $^4I_{15/2}$ ground state. We measured the lifetime of the lower state of SR by the time constant of the change in the absorption from the lower state of SR to the second lowest Stark level of the $^4I_{9/2}$ state ($\lambda = 802$ nm). Just after an SR pulse is generated, the population of the lower state of SR suddenly increases, and it results in the sudden increase of the absorbance. Then the absorbance decreases due to the population decay from the lower state of SR to the ground state. The lifetime of the lower state of SR is estimated to be roughly 400 ns from the exponential fit to the absorbance.

APPENDIX B: IDENTIFICATION OF THE OBSERVED PULSES AS SUPERRADIANCE

In the main text of this paper, we identified the observed optical pulses as superradiance (SR) based on the following observations: (i) short pulse duration, (ii) sech-squared pulse shape, (iii) relationship between pulse duration and height, and (iv) relationship between pulse area and height. Here we discuss in more detail.

The FWHM duration of the observed pulses is $\mathcal{O}(10\,\text{ns})$. The emission process is accelerated by a factor of 10^6 compared to the lifetime of the higher state of the transition (~ 10 ms). The characteristic time of SR T_R is longer than $\mathcal{O}(1\text{ns})$. Considering a numerical factor needed to convert T_R to the pulse duration and ambiguity in γ (radiative decay rate), the observed pulse duration is consistent with SR.

The observed pulse shown in Fig. 2(c) can be fit well by the sech-squared function $A \times \text{sech}^2((t - t_0)/B)$, with A, B, and t_0 as the free parameters. If the macroscopic polarization (coherence) develops homogeneously over the target ($L \ll cT_R$), the generated optical pulses go out of the sample so fast that they cannot be reabsorbed by target ions. On the other hand, the target length is required to be much longer than a threshold length L_T, which is derived from the requirement that the macroscopic dipole has to develop within a decoherence time T_2 [19]. This requirement is satisfied because intense optical pulses are indeed observed. The solution of the Maxwell-Bloch equations [2] reduces to a sech-squared function without any ringings in the condition where $L_T \ll L \ll cT_R$. This condition is satisfied in our system.

Fluctuations of the peak height, pulse duration, and photon number are large due to the stochastic nature of SR. Figure 5(a) is the relationship between a peak height and a pulse duration. The blue circles represent the average of pulse duration in a certain peak height range. The pulse duration increases with decrease in the peak height. According to the spatially homogeneous solution of the Maxwell-Bloch equations, the pulse duration ($\propto 1/N$) is inversely proportional to the square root of the peak height ($\propto N^2$), where N is the number of photons in a single pulse. The red solid line is the power fit of (duration) $= A \times$ (height)$^\alpha$ to the data, with A and α as the free parameters. The fitting result gives the index $\alpha = -0.60 \pm 0.01$, which is not significantly different from
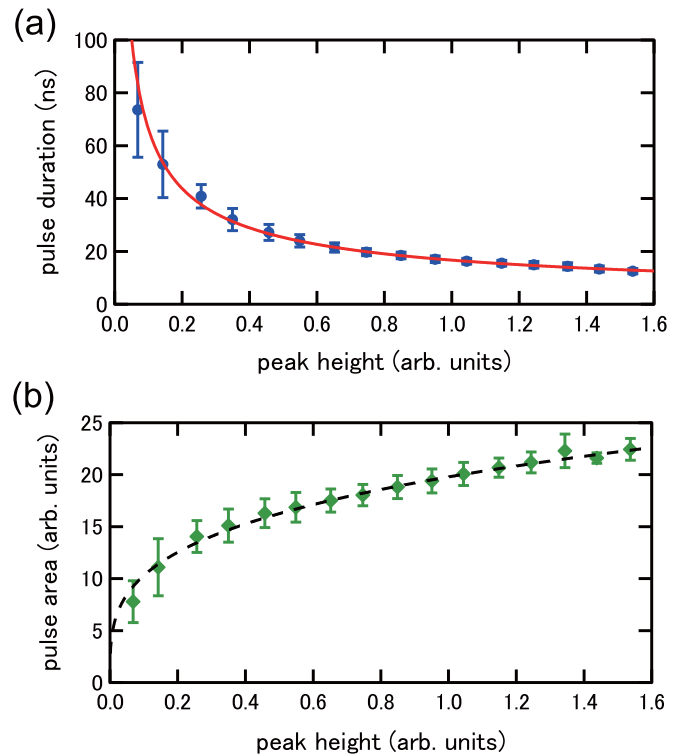

FIG. 5. (a) Relationship between pulse duration and peak height of each pulse. The data points are taken only after $t = 10$ ms. The blue circles represent the average of pulse duration in a certain peak height range. The error bars indicate the standard deviations, not the statistical errors. The red solid line is the power fit of (duration) $= A \times$ (height)$^\alpha$ to the data. (b) Relationship between pulse area and peak height of each pulse. The green diamonds and the error bars represent the average of pulse area in a certain peak height range and the standard deviations, respectively. The black dashed line is the power fit of (area) $= A \times$ (height)$^\alpha$ to the data.

-0.5 of the spatially homogeneous solution. Here the error is scaled so that the reduced χ^2 value is unity.

Figure 5(b) is the relationship between a peak height and a pulse area. The pulse area is proportional to the total emitted photon number. The green diamonds represent the average of the pulse area in a certain peak height range. The pulse area increases together with the peak height. According to the spatially homogeneous solution, the emitted photon number ($\propto N$) is proportional to the square root of the peak height ($\propto N^2$). The black dashed line is the power fit of (area) $= A \times$ (height)$^\alpha$ to the data, with A and α as the free parameters. The fitting result gives the index $\alpha = 0.28 \pm 0.01$, where the error is scaled so that the reduced χ^2 value is unity. The value of α is somewhat deviated from 0.5 of the spatially homogeneous solution, but the expected relationship between a peak height and a pulse area is considered to hold approximately. The result also supports the validity of the spatially homogeneous solution in that it deviates further from the value for the spontaneous emission ($\alpha = 1$, as mentioned later).

Because of the realistic experimental condition, it is possible that the results deviate from the simplified model, where the deexcitation process starts from a complete population inversion and the number of the excited ions are constant.

The source of the deviations from the spatially homogeneous solution is not clear currently. On the other hand, in Ref. [10], the authors explained the relationship between the peak photon emission rate and the observed photon number with the assumption that the observed photon number is greater than the number of Er^{3+} ions participating in the macroscopic state due to the single pass gain through the inverted medium. Our result in Fig. 5 can also be fit by the functions derived in their model.

The pulses we observed are consistent with the spatially homogeneous solution of the Maxwell-Bloch equations. Here we exclude another possibility of accelerating the deexcitation process, that is amplified spontaneous emission (ASE). Even if coherence is not sufficiently developed, spontaneous emission is amplified as the radiation propagates through an inverted medium. First, the observed pulse shape is different from that of ASE. The duration of the observed pulses is 20 ns on average, which is close to the order of the shorter limit of

T_R $\mathcal{O}(1\text{ns})$. The ASE pulse duration is expected to be much longer than T_R. The standard deviation of the observed pulse duration is 5 ns, which is much smaller than the variation of the ASE pulse duration. In ASE, CW components comparable to the pulse components are also present [21]. In our experiment, however, the CW component of the photons emitted in the forward direction is negligibly small with respect to the pulse component. Second, the relationship between the pulse area and height is different from that of ASE. In the case of spontaneous emission, the peak photon emission rate is proportional to the emitted photon number. This case corresponds to $\alpha = 1$ in $(\text{area}) = A \times (\text{height})^\alpha$. In the case of ASE, the index α is expected to be between 0.5 (SR) and 1 (spontaneous emission). Our result ($\alpha = 0.28 \pm 0.01$) is different from this range and is close to the limit of SR. These results suggest that the observed pulses are not ASE. From the above discussions, it is possible to identify that the pulses we observed are SR.

---

[1] R. H. Dicke, Coherence in spontaneous radiation processes, Phys. Rev. **93**, 99 (1954).

[2] M. Benedict, A. Ermolaev, V. Malyshev, I. Sokolov, and E. Trifonov, *Super-radiance: Multiatomic Coherent Emission* (Taylor & Francis Group, London, 1996).

[3] N. Skribanowitz, I. P. Herman, J. C. MacGillivray, and M. S. Feld, Observation of Dicke superradiance in optically pumped HF gas, Phys. Rev. Lett. **30**, 309 (1973).

[4] M. Gross, C. Fabre, P. Pillet, and S. Haroche, Observation of near-infrared Dicke superradiance on cascading transitions in atomic sodium, Phys. Rev. Lett. **36**, 1035 (1976).

[5] N. Carlson, D. Jackson, A. Schawlow, M. Gross, and S. Haroche, Superradiance triggering spectroscopy, Opt. Commun. **32**, 350 (1980).

[6] R. Florian, L. Schwan, and D. Schmid, Superradiance and high-gain mirrorless laser activity of O^-_2-centers in KCl, Solid State Commun. **42**, 55 (1982).

[7] G. Rainò, M. A. Becker, M. I. Bodnarchuk, R. F. Mahrt, M. V. Kovalenko, and T. Stöferle, Superfluorescence from lead halide perovskite quantum dot superlattices, Nature (London) **563**, 671 (2018).

[8] A. Angerer, K. Streltsov, T. Astner, S. Putz, H. Sumiya, S. Onoda, J. Isoya, W. J. Munro, K. Nemoto, J. Schmiedmayer *et al.*, Superradiant emission from colour centres in diamond, Nat. Phys. **14**, 1168 (2018).

[9] K. Cong, Q. Zhang, Y. Wang, G. T. Noe, A. Belyanin, and J. Kono, Dicke superradiance in solids, J. Opt. Soc. Am. B **33**, C80 (2016).

[10] C. Braggio, F. Chiossi, G. Carugno, A. Ortolan, and G. Ruoso, Spontaneous formation of a macroscopically extended coherent state, Phys. Rev. Res. **2**, 033059 (2020).

[11] T. Böttger, C. W. Thiel, R. L. Cone, and Y. Sun, Effects of magnetic field orientation on optical decoherence in Er^{3+} : Y_2SiO_5, Phys. Rev. B **79**, 115104 (2009).

[12] C. Simmon, M. Afzelius, J. Appel, A. B. de la Giroday, S. Dewhurst, N. Gisin, C. Hu, A. Jelezko, S. Kröll, J. Müller *et al.*, Quantum memories: A review based on the European integrated project "Qubit Applications (QAP)", Eur. Phys. J. D **58**, 1 (2010).

[13] M. Zhong, M. P. Hedges, R. L. Ahlefeldt, J. G. Bartholomew, S. E. Beavan, S. M. Wittig, J. J. Longdell, and M. J. Sellars, Optically addressable nuclear spins in a solid with a six-hour coherence time, Nature (London) **517**, 177 (2015).

[14] M. Rančić, M. P. Hedges, R. L. Ahlefeldt, and M. J. Sellars, Coherence time of over a second in a telecom-compatible quantum memory storage material, Nat. Phys. **14**, 50 (2018).

[15] N. Sasao and M. Yoshimura, New method of galactic axion search, The European Physical Journal C **78**, 949 (2018).

[16] H. Hara and M. Yoshimura, Raman stimulated neutrino pair emission, The European Physical Journal C **79**, 684 (2019).

[17] H. Hara, A. Yoshimi, and M. Yoshimura, Parity violating magnetization at neutrino pair emission using trivalent lanthanoid ions, Phys. Rev. D **104**, 115006 (2021).

[18] T. Böttger, Y. Sun, C. W. Thiel, and R. L. Cone, Spectroscopy and dynamics of Er^{3+} : Y_2SiO_5 at 1.5 μm, Phys. Rev. B **74**, 075107 (2006).

[19] R. Bonifacio and L. A. Lugiato, Cooperative radiation processes in two-level systems: Superfluorescence, Phys. Rev. A **11**, 1507 (1975).

[20] F. Sanchez, P. Le Boudec, P.-L. François, and G. Stephan, Effects of ion pairs on the dynamics of erbium-doped fiber lasers, Phys. Rev. A **48**, 2220 (1993).

[21] M. S. Malcuit, J. J. Maki, D. J. Simkin, and R. W. Boyd, Transition from superfluorescence to amplified spontaneous emission, Phys. Rev. Lett. **59**, 1189 (1987).